Build-to-Last: Strength to Weight 3D Printed Objects

Lin Lu[1]* Andrei Sharf[2] Haisen Zhao[1] Yuan Wei[1] Qingnan Fan[1] Xuelin Chen[1]
Yann Savoye[2] Changhe Tu[1] Daniel Cohen-Or[3] Baoquan Chen[1]†

[1] Shandong University [2] Ben-Gurion University [3] Tel Aviv University

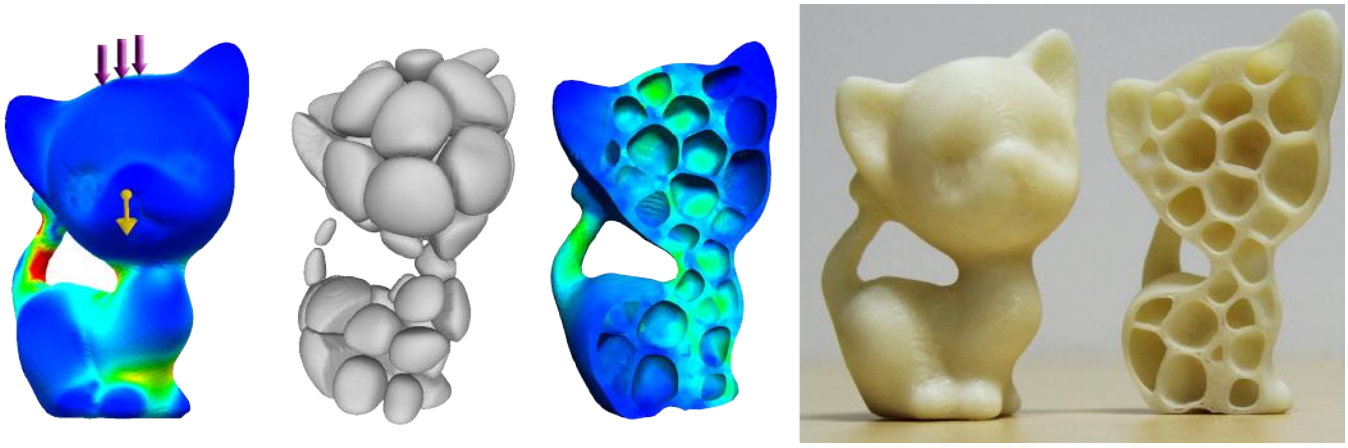

Figure 1: *We reduce the material of a 3D kitten (left), by carving porous in the solid (mid-left), to yield a honeycomb-like interior structure which provides an optimal strength-to-weight ratio, and relieves the overall stress illustrated on a cross-section (mid-right). The 3D printed hollowed solid is built-to-last using our interior structure (right).*

Abstract

The emergence of low-cost 3D printers steers the investigation of new geometric problems that control the quality of the fabricated object. In this paper, we present a method to reduce the material cost and weight of a given object while providing a durable printed model that is resistant to impact and external forces.

We introduce a hollowing optimization algorithm based on the concept of *honeycomb-cells* structure. Honeycombs structures are known to be of minimal material cost while providing strength in tension. We utilize the Voronoi diagram to compute irregular honeycomb-like volume tessellations which define the inner structure. We formulate our problem as a *strength–to–weight* optimization and cast it as mutually finding an optimal interior tessellation and its maximal *hollowing* subject to relieve the interior stress. Thus, our system allows to *build-to-last* 3D printed objects with large control over their strength-to-weight ratio and easily model various interior structures. We demonstrate our method on a collection of 3D objects from different categories. Furthermore, we evaluate our method by printing our hollowed models and measure their stress and weights.

CR Categories: I.3.5 [Computer Graphics]: Computational Geometry and Object Modeling—Curve, surface, solid, and object representations;

Keywords: 3D printing technologies, solid object hollowing, porous structure design, volume-Voronoi shape

*e-mail:lulin.linda@gmail.com
†e-mail:baoquan.chen@gmail.com

Links: DL PDF

1 Introduction

Recent years have seen a growing interest in 3D printing technologies, capable of generating tangible solid objects from their digital representation. Typically, physically printed objects are built by successively stacking cross-section layers of powder-based material. Layers are generated through fused-deposition modeling and liquid polymer jetting. Hence, the production cost of the resulting model is directly related to the volume of material effectively employed in the printing process. In turn, this can be a costly operation for large and complex models. To mitigate this, few methods have recently focused on the problem of designing cost effective 3D shapes by reducing their interior material. In their recent work, Wang et al. [2013] introduce one of the first cost-effective printing strategies using skin frame structures to support the shape's interior. Recent material-aware 3D printing techniques [Stava et al. 2012; Prévost et al. 2013; Zhou et al. 2013; Umetani and Schmidt 2013] describe object breakability, stress and fatigue-related collision as challenging issues that are very important to handle for 3D printing.

Our work draws inspiration from the Voronoi structure. Given a

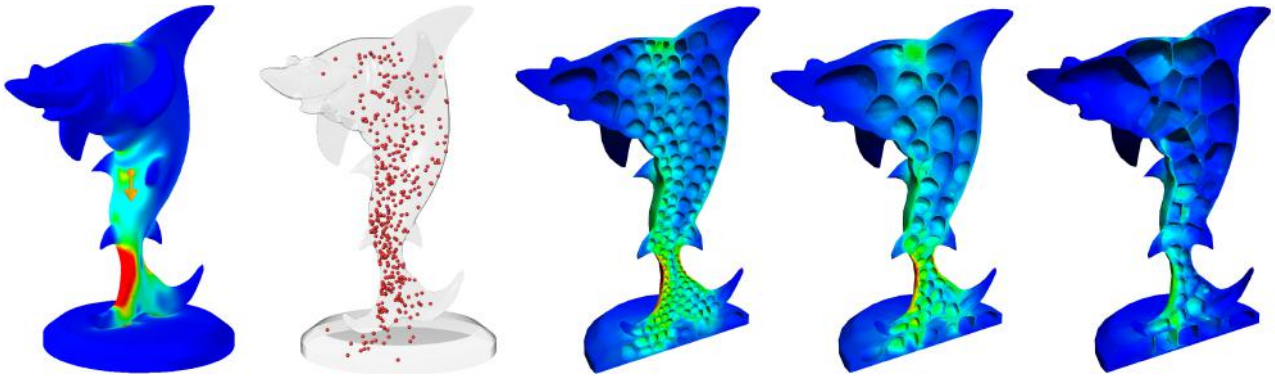

Figure 2: *Given a 3D shape of a shark and external forces we compute an initial stress map (a) and generate a corresponding interior point distribution (b). We compute the lightest interior that sustains the given stress through an optimization process. We show here two steps (c-d) of the optimization and an optimal strength-to-weight ratio in (e).*

set of sites, the Voronoi diagram defines a space partitioning into closed-cells of nearest regions with respect to the sites [Voronoi 1908]. As the number of sites increases, Voronoi cells converge to hexagonal honeycomb-like shapes [Bronstein et al. 2008], producing a structure of high strength-to-weight ratio for any material [Wilson 1990]. In our work, we utilize an adaptive centroidal Voronoi diagram to partition the shape's interior volume into honeycomb like cells. The cells are distributed with respect to a density function defined by a stress map, where each cell is governed by its centroid.

We introduce a novel algorithm for material distribution and interior structure optimization which accounts for shape strength with respect to exterior forces. The object's stress is defined as a measure of the structural failure of a material with respect to load and force. Thus, we cast the optimization problem as mutually finding an optimal tessellation of the interior and its maximal *hollowing* while sustaining interior stress. We compute honeycomb-like tessellations using an adaptive centroidal Voronoi partition of the interior volume. Hollowing is defined as the porosity inside each Voronoi cell which consequently reflects the density of the shape's interior material. Given an arbitrary input object, we reduce its material amount, providing lightweight solids with an organic interior structure that is durable and resistant to bending and breaking. Our method allows easy control to trade off shape's strength vs. material while preserving its boundary surface geometry.

We formulate our material-saving optimization as the solution of a hollowing (i.e., material removal) process of a shape's interior under stress and exterior forces constraints. We represent hollowing as an aggregation of harmonic fields defined on the Voronoi tessellation of the objects' volume. Each harmonic field defines the amount of hollowness within each Voronoi cell. We model the stress, strain and exterior forces and solve to find the optimal hollowing parameter while sustaining the stress.

Our method makes the following contributions:

- we introduce a novel material optimization framework with respect to the interior and exterior forces. Our algorithm maximizes the hollowing of a Voronoi-guided porous structure while sustaining a given stress.
- we adapt the centroidal Voronoi as a generative model for 'like-natural' honeycomb interior structures. This leads to a high strength-to-weight ratio.
- our technique allows an easy control of the trade-off between the object strength and interior amount of material.

2 Related Work

Recent years have shown a growing interest in 3D printing technologies, capable of generating tangible solid objects from their digital representation. In practice, 3D printers are a powerful yet affordable commercial solution to popularize the self-prototyping of custom-designed physical objects. This accessibility to flexible design has already propelled creativity in footwear fashion and opened new horizons in computation-assisted fabrication in medicine and aerospace. Thus, the 3D printing revolution has introduced novel problems and challenges in the fields of geometry processing and modeling, towards the purpose of sustainable 3D printability.

Our literature review focuses on two areas which are nowadays rapidly evolving, namely, *Computational Fabrication* and *Lightweight Structure Synthesis*. We narrow the discussion to the context of the strength-to-weight problem for printable 3D objects.

Computational Fabrication. Recently, significant efforts have been spent on establishing physically-fabricated prototypes and manufactured objects using 3D printing like animatronic mold [Zhu et al. 2012; Bickel et al. 2012]. Similarly, the work by Li et al. [2013] proposed a Kinect-based method for 3D printing of self-portraits miniatures from watertight surfaces. Such fabrication techniques introduced various printability assessment criteria like local thickness [Telea and Jalba 2011].

Researchers have also addressed multi-material 3D printing [Vidimče et al. 2013], as well as inner material distribution optimization [Chen et al. 2013]. Bickel et al. [2010] formulate the stress-strain relationship in a finite-element model to fabricate multi-material objects with inhomogeneous behavior.

Several methods facilitate the structural design optimization for deformable characters [Skouras et al. 2013] and skinned mechanical objects [Coros et al. 2013; Calì et al. 2012], addressing the problem of 3D-printing of joints. Bacher [2012] presents an algorithm to estimate structurally optimal articulated characters for strength using printable ball-and-socket joints.

Researches have also focused on introducing fabrication-oriented design for a large range of applications such as custom-shaped inflatable ballons [Skouras et al. 2012], 2D material cutout [Rivers

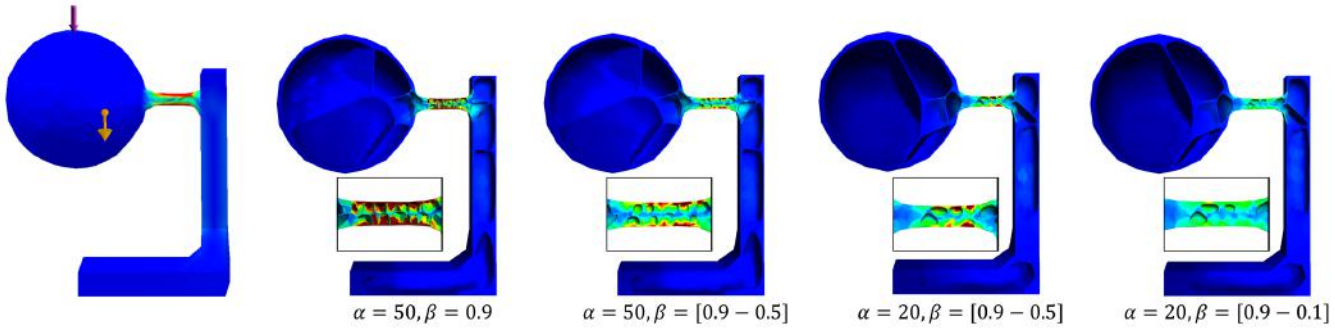

Figure 3: *Optimization of the interior structure of a hanging-ball. (a) the initial objects displayed with its applied force and stress map. (b) optimization starting from a large α and β (i.e., dense tessellation and light volume). In the inner loop, we locally reduce β to relieve stress (c). In the outer loop, we reduce α to further improve sustainability (d). Repeating this process yields an optimal strength-to-weight ratio (e).*

et al. 2012], mechanical automata [Ceylan et al. 2013] and architectural design [Pottmann 2012].

Lightweight Structure Synthesis. Structure synthesis and scaffolding, have been extensively explored in tissue engineering and computer-aided design [Hollister 2005; Schroeder et al. 2005]. Our work is inspired by the technique of Kou et al. [2010] designing irregular-shaped pores using Voronoi tessellation and B-Spline. Since the iso-porous model is suitable for additive manufacturing [Khoda et al. 2013], our work reformulates and generalizes this nature-inspired porous scaffolding approach for the purpose of 3D object hollowing optimization.

The field of structural engineering has paid a lot of attention to the *structural rigidity* [Crapo and Whiteley 1993; Rosenberg 1980], structural optimization [Haftka and Grandhi 1986] and structural stability [Crapo 1979]. Engineers have developed lightweight structural cores (i.e. , honeycomb, balsa and foam) to reduce weight and enforce strength [Kindinger 2001]. In particular, honeycomb cores are material-efficient thanks to their hexagonal cell configuration [Wilson 1990]. Outstandingly, the hexagon pattern is one nature's most efficient structure with the highest strength-to-weight ratio for any known material. In its closed-packed form, the hexagonal-patterned lattice is the steady-state configuration of all Voronoi diagrams.

The idea of cost-effective 3D printing by reducing the used material has been recently introduced in [Wang et al. 2013]. In their work, the solid interior of an object is replaced by truss scaffoldings. Their structure synthesis is optimized iteratively to reduce the truss structure while accounting for several physical and geometrical constraints. In contrast, our method is based on a global optimization of the strength-to-weight ratio. To overcome lack of stability, Prevost et al. [2013] carve the interior volume to improve its equilibrium. Similarly to us, they define the shape's interior modification as an energy minimization problem to optimize balance. Nevertheless, their goal is to make-it-stand while ours is to build-to-last.

Reducing the object's interior material is an important property for reducing 3D printing costs and durance. Nevertheless, it should be tightly coupled with strength characteristics of the object to guarantee the physical object durability. In their work, Zhou et al. [2013] identify structural problems in objects by solving a constrained optimization problem. To do this, they build a weakness map to measure the shape response to worst-case external pressure. In our work, we incorporate the structure stress as a function of the local hollowing in the optimization process.

Similar to us, Stava et al. [2012] improve the structural strength of printable objects through modification of their interior. They define an iterative optimization process where supporting struts, thickening and hollowing are applied to sustain stress and grip forces. In contrast, we formulate the strength-to-weight optimization as a global constrained optimization and formulate stress as a hollowing functional approximation.

3 Overview

Given a 3D object represented by its boundary surface mesh, our method hollows its volume, yielding a supportive interior structure. The method controls the balance of weight and strength of the printed model such that the printed shape contains a minimal amount of material, which can resist a prescribed external force and imposed interior load.

From the input 3D shape, exterior forces and gravity, we initially compute a stress map that represents the stress at each internal point (Figure 2(a)). We regard the stress map as a continuous volumetric density map for which we generate a locally varying point distribution that reflects the underlying density map (Figure 2(b)).

The initial inner structure is then defined by constructing an adaptive centroidal Voronoi tessellation which partitions the object's interior into a set of closed-cells. We then construct a harmonic field inside each Voronoi cell and define the pore function as the isosurface corresponding to a given isovalue inside this field. The pore is computed by explicitly extracting its surface and carving out the inner volume (Figure 2(c)).

Essentially, the construction of the pore-based inner structure is controlled by two parameters: α, defining the total number of inner cells and, β defining the hollowing amount inside each cell. Thus, increasing the value of α yields a denser structure while increasing β raises the hollowing (pores size). Intuitively, smaller pores imply more inner material, and thus heavier objects. Normally an inner structure that is less hollow implies more strength.

In our work, we optimize the α and β levels to increase the strength-to-weight ratio. To optimize this ratio, our algorithm searches for the lightest interior that can sustain a prescribed force F. Thus, we define for each cell a hollowing level $\{\beta_0, ..., \beta_n\}$. Since our functional space is non-monotonic, we search for an optimal α, β values by an adaptive Monte Carlo optimization approach (Figure 2(c-e)).

Starting from an initial guess, we locally optimize β to relieve stress

in an iterative manner. We take a spatially-varying approach, where only regions with stress higher than the material's *"yielding point"* are refined, generating a spatially-varying β set. In short, the yielding point defines a stress threshold when the material begins to deform. We further optimize our structure by locally optimizing α for a given β. Figures 2(c-e) display three optimization iterations.

4 Technical Details

Stress-FEM Processing Our input consists of a 3D object denoted by $\mathcal{S}$, which is positioned in a physical environment consisting of gravity, user defined forces, and fixtures supporting parts. We compute an initial stress map using the OOFEM finite element library [Patzak and Rypl 2012]. To compute the stress using FEM, we tetrahedralize the object's interior using Tetgen library [Si 2007].

The stress is computed using the per-element stiffness matrices encoding the flexibility of each tet-element. We assume a Hooke's linear elastic model and a single uniform isotropic material. Aggregating all per-element stiffness matrices and forces, yield a displacement field. Thus strain tensor is built from the Jacobian of the displacement field for each element, and stress tensor is the linear combination of the elasticity matrix and strain tensor [Wicke et al. 2007]. This yields a continuous stress map defined everywhere within the volume of the shape (see Figure 2(a)).

Stress-map Adaptive Centroidal Voronoi Next, we distribute a set of sites inside the object's volume in accordance with the density map defined by the stress. Sites propagate through an error-diffusion process analogous to halftoning, where higher stress values indicate a denser sites dispersion. The initial number of sites denoted by α dictates the overall site density (see Figure 4 for distributions with different α).

For the input boundary surface $\mathcal{S}$ and a given quantity of $\alpha = n$ sites $\{s_i\}_{i=1}^{n}$ defined in the interior domain of $\mathcal{S}$, a *Voronoi tessellation* of $\mathcal{S}$ is defined to be the collection of *Voronoi cells* $\{\Omega_i\}_{i=1}^{n}$ of the sites, where

$$\Omega_i = \{\mathbf{x} \in \mathcal{S} | \, \|\mathbf{x} - s_i\| \leq \|\mathbf{x} - s_j\|, \forall j \neq i \, \},$$

and $\| \cdot \|$ denotes the Euclidean norm. A Voronoi tessellation is called a *centroidal Voronoi tessellation* (CVT) [Du et al. 1999] if each site coincides with the centroid of its Voronoi cell, where the centroid $\mathbf{c}_i$ of its Voronoi cell Ω_i is defined as

$$\mathbf{c}_i = \frac{\int_{\mathbf{x} \in \Omega_i} \rho(\mathbf{x}) \mathbf{x} \mathrm{d}\sigma}{\int_{\mathbf{x} \in \Omega_i} \rho(\mathbf{x}) \mathrm{d}\sigma},$$

in which $\mathrm{d}\sigma$ is the area differential, and $\rho(\mathbf{x})$ is the density function over the domain $\mathcal{S}$ corresponding to the stress map. We use Lloyd's method [Lloyd 1982] to iteratively compute the CVT.

CVT results in two types of Voronoi cells, convex inner cells and boundary cells that may be concave due to their clipping with the boundary surface mesh $\mathcal{S}$ (see Figure 5).

Harmonic Porous Extraction In order to hollow a Voronoi cell, we compute a harmonic distance field inside each cell which defines an implicit representation of the porous. Thus, the hollowing parameter expresses an iso-value in the harmonic field and the corresponding level set defines the porous surface. We define a harmonic scalar function $\varphi_i : \mathbb{R}^3 \mapsto \mathbb{R}$ for each Voronoi cell Ω_i, satisfying Laplace's equation $\nabla^2 \varphi_i = 0$ with two Dirichlet boundary

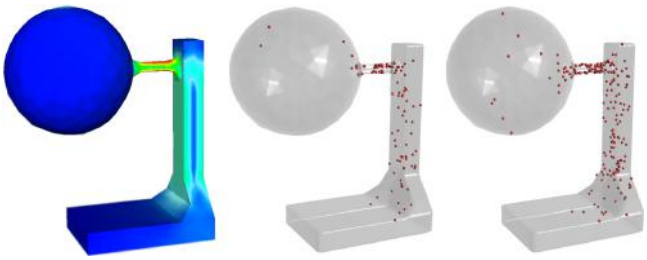

(a) (b) (c)

Figure 4: *Interior points distribution according to stress map (a) with 100 (b) and 200 (c) sites.*

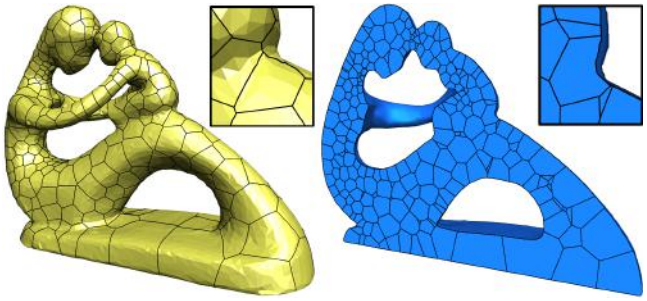

(a) (b)

Figure 5: *The centroidal Voronoi boundary and inner cells. Note the non-convex cell at the baby's lower back.*

conditions B_0 and B_1, such as:

$$\begin{cases} \nabla^2 \varphi \, (\mathrm{p}) = 0 \ , \ \forall \mathrm{p} \notin (B_1 \cup B_0) \\ \varphi \, (\mathrm{p}) = \kappa \ , \ \forall \mathrm{p} \in B_1 \\ \varphi \, (\mathrm{p}) = 0 \ , \ \forall \mathrm{p} \in B_0 \end{cases} \quad (1)$$

where B_1 is the condition defined as the subset of voxels on the cell boundary $\partial\Omega_i$, and B_0 is the condition defined as the voxel containing the cell's centroid. We multiply the value for boundary cells B_1 by a factor κ related to negative average curvature as surface special treatment. For negative curvature, κ is the absolute average curvature, and 1 otherwise (see Figure 6(c)).

We clip Voronoi cells with the object's surface [Yan et al. 2013], to guarantee that the structure is completely inside. Due to this clipping, some Voronoi cells intersecting the object's surface may consist concavities which intersect the harmonic field. Therefore, we modify the boundary condition of voxels with negative curvature such that it pushes away the field (see Figures 5 and 6) .

In practice, we express the Laplacian operator over the voxel grid, discretizing the volume of the given Voronoi cell. We solve this system via a volumetric heat diffusion process [Li et al. 2007]. Next, for a given iso-value, we compute the explicit triangular mesh. Additionally, we tetrahedralize the space bounded by the pore's exterior and the boundary of its Voronoi cell (with Tetgen).

Strength-to-weight Optimization We formulate the strength-to-weight maximization as a stochastic optimization of two parameters: α exclusively controlling the site distribution density i.e., the number of Voronoi cells in the volume tessellation; and $\beta = \{\beta_0, ..., \beta_n\}$ ($\beta_i \in [0, 0.9]$) controlling the hollowing value in each cell. Essentially both parameters cooperatively govern the interior mass distribution and object's strength.

Intuitively, decreasing hollowness in each cell (β), the object becomes heavier and also stronger, enabling higher loads to be applied (Figure 3(b-c)). Nevertheless, heavier regions may increase the object's interior load, possibly increasing stress in other regions. Additionally, the decrease of α, results in the object being stronger and heavier (Figure 3(c-d)). We explain this phenomena, as larger cells, consists of larger cell walls which are more elastic (with larger attenuation) and thus can sustain more stress. In terms of their weight, larger boundary cells, typically consists larger concavities and therefore requiring more material.

This leads to the observation that the strength-to-weight ratio behavior is highly non-linear and non-monotonic which justifies the need of a complex optimization scheme. To solve it, we devise an efficient local optimization coupled with an adaptive Monte-Carlo stochastic sampling.

Denote $W_{\mathcal{S}}(\alpha, \beta)$ as the volume function of the shape $\mathcal{S}$ with parameters α, β. To optimize the strength-to-weight ratio our method searches for the lightest interior, which can sustain a predefined stress. This search can be formulated into a constrained optimization, as follows:

$$\underset{\alpha,\beta}{\operatorname{argmin}} W_{\mathcal{S}}(\alpha, \beta) \;\; s.t. \;\; SM(\mathcal{S}, F) < \chi$$

where $SM(\mathcal{S}, F)$ is the stress map computed by applying the forces F on $\mathcal{S}$. χ is the yielding point of a specific material (by default we use $\chi = 4.1e^7 N/m^2$ for plastic).

We independently solve the optimization problem for α and β using two loops. In the inner loop, we optimize β keeping α constant, and in the outer loop we optimize α. Our algorithm alternates between the two optimizations until convergence to a minima. Note that it is possible to solve only for α or β, leading to a light interior that sustains a predefined stress. Nevertheless, this solution is only a local minimum. Reducing both the number of cells in the tessellation as well as their interior mass provides more degrees of freedom in the optimization and leads to a lighter and more compact interior structure (see Figure 7).

We start with an initial guess of α^0 and then compute the Voronoi tessellation corresponding to the distribution of α^0 sites. The selection of α^0 depends on the complexity of the given shape and the initial stress distribution; based on our experiments $\alpha^0 = 100$ is enough for most models. In the inner loop, we search for the largest hollowing value of the Voronoi cells that sustains the predefined stress. Starting from a maximal hollowed cells, i.e., $\beta^0 = 0.9$ uniformly, we increase the per-cell mass (decreasing β) in regions of high stress. Specifically, given a set of hollowing values $\{..., \beta_i^0, ...\}$, we are able to evaluate the corresponding stress map ($SM^0(\mathcal{S}, F)$). Next, we search for cells $\Omega_i \in \mathcal{S}$ with a stress value above the yielding point $\bigcup\{\Omega_i\} \; SM^0(\Omega_i, F) > \chi$ and relieve the stress there by locally reducing their hollowing value: $\beta_i^1 = \beta_i^0 - \epsilon$, where $\epsilon = 0.1$. We repeat this process until stress in all cells is below yielding point.

By observation, our functional space is non-monotonic due to the non-linear nature of stress and material (see Figure 7). Thus, by locally increasing the per-cell mass to relieve stress may add an interior load factor enforcing additional stress in other regions. Furthermore, we leverage stress both by decreasing β and α however at a cost of increasing mass non equivalently.

We incorporate a Monte Carlo stochastic sampling approach to avoid local minima and improve our optimization iterations. Thus, we run several Monte Carlo iterations, sampling in the sliding windows around current β values. This process refines our computation and narrow down locally to optimal values. This approach yields a spatially-varying hollowing, where only regions with higher stress are refined.

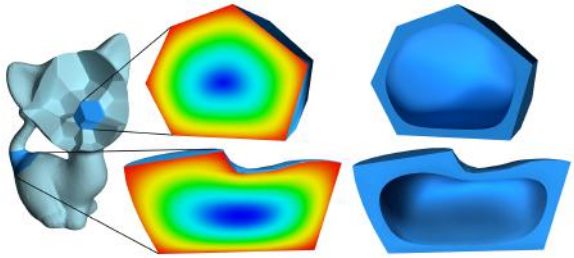

(a) (b) (c)

Figure 6: *Harmonic porous carving. For two highlighted interior Voronoi cells of a 3D kitten (a), we show in a cross section the harmonic distance field (b) and the carved result for $\beta = 0.7$ (c).*

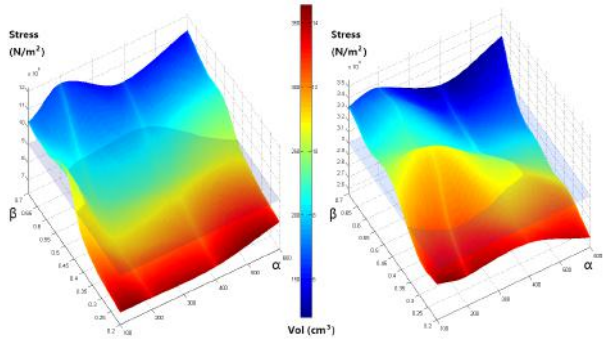

(a) (b)

Figure 7: *The functional space of fertility (left) and shark (right). Stress and volume are given as function of α and β. Our constraint optimization searches for the lightest volume (color) with overall stress below a given yielding point (intersecting transparent plane).*

In the outer loop, we aim to reduce the number of cells to obtain a more compact packing of cells and further relieve stress. For a given near-optimal β and initial guess α^0, we merge together neighbor cells that share a similar hollowing value, by removing them and replacing with a single site with the same value. Consequently, we locally refine the Voronoi diagram by Voronoi deletion and insertion operations obtaining an optimal α^1.

We repeat inner loop to further refine β given the updated Voronoi structure. This process repeats until convergence or until the overall mass does not significantly change from one iteration to another.

5 Results

We have computed the optimal strength-to-weight interior structures for various 3D objects. Models were selected from different categories (e.g. sculpture, CAD, mechanics, medical and etc.), consisting of a wide range of typical features and stress distribution. For evaluation purposes, we run *real-world tests*, in which we measure the physical properties of weight and sustained stress for a 3D printed object and check against our computed values.

Optimization Figure 3 shows our interleaved optimization of α and β through alternate optimization iterations. To clearly illustrate the inner structures, we start with a relative small value $\alpha^0 = 50$, and maximally hollowed $\beta^0 = 0.9$ (b), we compute in the inner

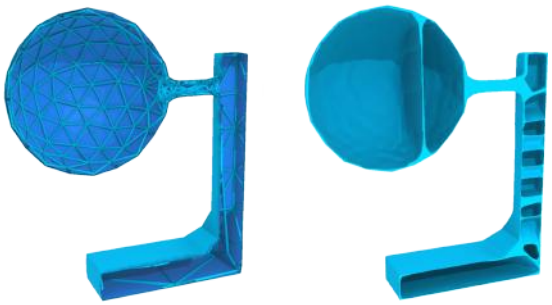

Figure 8: *In comparison to the skin-frame algorithm (left), ours (right) is lighter and sustains significantly higher stress.*

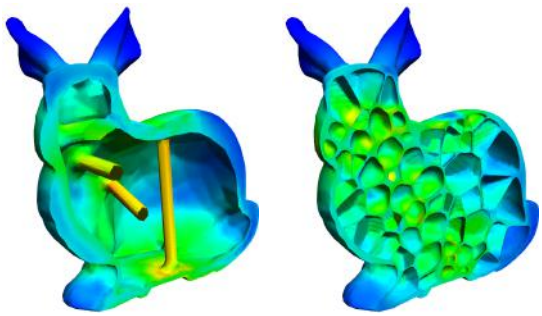

Figure 9: *Comparing the struts structure (left) with that produced from our method (right), for the same applied forces, our model is significantly lighter.*

loop the optimal β set, defining the lightest interior to sustain the given stress (c). Next, in the outer loop we can further relieve stress by reducing α (d). Thus, we merge together neighboring cells with similar β value, reducing the number of cells which in turn improves strength (here weight increased).

We have tested our algorithm on a PC with a 3.2GHZ Core CPU, 8GB RAM, running Windows OS. Our optimization runs on average 15 iterations and maximum of 22 iterations. The number of outer loop iterations were 20% and inner 80%. The optimization time bottle-neck was the stress map computation requiring the computation of an FEM structure and the physical simulation. Since FEM is shape aware our optimization time corresponds to the shape complexity and also the carving level. The more hollow, the more time consuming was the stress map computation due to the thin structures supporting the shape. The total time for the optimization process stayed below 2 hours and on average of 40 minutes. In most cases our parameter range were in the optimum $\alpha = 30$ and $\beta = [0.9 - 0.1]$

Comparisons In Figure 8, we compare our method with the skin-frame structure of Wang et al. [2013]. Running our method on the 3D hanging-ball, resulted in a stronger and lighter object. Our optimally hollowed model can sustain an external force (positioned vertically down from the top) of $20N$ with a mass of $92.5g$ ($\alpha = 20, \beta = [0.9 - 0]$). Their reported skin-frame model with the same force direction sustains only $5N$ with a slightly heavier a mass of $109.3g$.

In Figure 9, we compare our results with the struts structure [Stava et al. 2012]. In their evaluation, they applied four predefined pinch grips one a bunny model with four inner struts. Their structure could resist $500N$ with a mass of $84.3g$. Using our algorithm, with the same force settings, the bunny resisted the same grip force of $500N$, however for a much lighter mass of $59g$.

Physical Test To evaluate the printability effectiveness of our honeycomb like interior structures, we 3D print our hollowed objects by a FORTUS 360mc printer using FDM© (Fused Deposition Modeling) technology. We use a plastic PC-ABS material with a *yield strength* of $4.1e7N/m^2$. In Figure 10, we show a collection of our build-to-last printed models as well as their interior.

Here we used a dissolvable substance for the support material in the cells, and dissolved it out by soaking the models in a solvent. The inner cells far from the boundary can be pierced by small holes that allow solvent to go in and empty the cells. Besides FDM, our proposed hollowing technique also works well for DLP (Direct Light Processing) and Stereolithography printers that incrementally add one polymer layer at a time, therefore no need for support material inside pores. However, we note that our method does not apply to SLS (Selective Laser Sintering) printers, because the object being printed is surrounded by unsintered powder all the time, such that the interior powder cannot be taken out.

We use an electromechanical universal testing machine (SANS CMT5105) to physically evaluate the strength of the printed models, as shown in Figure 11. The crosshead of the machine is controlled to move at a constant speed $1mm/min$ and outputs the constant compression force. The force value against the displacement of the crosshead is plotted synchronously.

We ran compression tests for two printed cups; one is Cup1, with a mass of $27.087g$ ($\alpha = 50, \beta = 0.9$), which is the intermediate result; the other is Cup2, with a mass of $27.551g$ ($\alpha = 50, \beta = [0.9 - 0]$), which is the optimal result. Cup1 got broken with the force $108.0N$; however, Cup2 can sustain $194.6N$. The results after broken by the crushing loads are displayed in Figure 12. (The process can be seen in the accompanying video.)

Evaluation To evaluate the performance of our strength-to-weight hollowing optimization we select 3D models, design and apply various forces on them and compute the minimal volume to sustain the resulting stress map. Figure 13 shows the result of our method on a collection of various models. We apply forces in different regions and of different size (left column). Starting from an initial tessellation with $\alpha^0 = 100$, which works well for all the models we tested, and a completely hollow interior $\beta = 0.9$ (mid-left column), we compute the stress map and relieve stress locally by decreasing hollowing (β) in the inner loop and decreasing cell density α in the outer loop (mid two columns). In the mid-right column we show an optimal strength-to-weight solution. The porous structure for the final results are shown in the rightmost column.

In Table 1, we summarize the various quantities for these models showing a significant weight reduction while objects strength was sufficient to sustain significant forces applied on them.

6 Conclusions

In this paper, we addressed the hard problem of hollowing solid objects while optimizing their strength-to-weight ratio. A novel optimization algorithm has been proposed to automatically select the near-optimal hollowing parameters which relieves stress while maximizing the strength-to-weight ratio. We demonstrate and evaluate the printability and strength of different 3D objects which are hollowed using our lightweight inner structure.

Our algorithm jointly utilizes a centroidal Voronoi tessellation, har-

Figure 10: *We build-to-last and 3D print our models as well as their hollowed honeycomb-like interiors. A standard key is as the size reference.*

Model	Solid Vol. (cm^3)	Result Vol. (cm^3)	Ratio $(\%)$	Stress (N/m^2)
Chair	719.24	472.03	65.6	4.00e7
Cup	214.4	89.33	41.7	4.01e7
Fertility	54.24	20.02	36.9	4.01e7
Hangingball	226.66	58.5	25.8	2.65e7
Horse	449.53	196.13	43.6	3.98e7
Kitten	125.07	50.79	40.6	2.57e7
Molar	15.22	9.64	63.3	4.05e7
Shark	130.42	43.4	33.3	3.90e7

Table 1: *Summary table for our results.*

monic distance field and a stochastic optimization for computing lightweight hollowed objects. A key advantage of our framework is its controllability of the optimization. It allows to compute the interior hollowed structure while adapting the structure density and its hollowness by simply adjusting two parameters. Our algorithm searches the optimal values for a set of predefined forces through an alternate optimization process.

Limitations and Future Work There are several remaining challenges raised from our work. Our stress computation is rather an approximation of the actual stress. Most importantly, we did not simulate the full physical phenomena due to the computational complexity it imposes. For example we did not consider in our stress computation the outside temperature, material fatigue and shape memory caused by forces. Furthermore, our optimization technique does not guarantee a global minima since it applies a local random sampling Monte-Carlo approach. Defining stress as a function of our hollowing parameter in a closed form would yield a global optimal solution. Nevertheless, efficient approximation of stress still remains an open problem.

A natural extension for our approach is to consider multi-material objects, thus performing a material-aware object hollowing optimization. This problem is challenging as it involves understanding multi-material interaction and its complex stress behavior. Another possible extension is towards 3D printing of articulated objects consisting of mechanical joints and functional parts.

Acknowledgements

We thank the reviewers for their valuable suggestions, Qiannan Li for video editing, and Maggie Chen for video narration. This work was partially supported by grants from NSFC (61202147, 61025012, 61332015, U1035004), Israel Science Foundation and European FP7. Lin Lu and Changhe Tu are also from Engineering Research Center of Digital Media Technology, Ministry of Education of PRC.

Figure 11: *Compression tests using a universal testing machine.*

References

BÄCHER, M., BICKEL, B., JAMES, D. L., AND PFISTER, H. 2012. Fabricating articulated characters from skinned meshes. *ACM Trans. Graph. 31*, 4 (July), 47:1–47:9.

BICKEL, B., BÄCHER, M., OTADUY, M. A., LEE, H. R., PFISTER, H., GROSS, M. H., AND MATUSIK, W. 2010. Design and fabrication of materials with desired deformation behavior. *ACM Trans. Graph. 29*, 4.

BICKEL, B., KAUFMANN, P., SKOURAS, M., THOMASZEWSKI, B., BRADLEY, D., BEELER, T., JACKSON, P., MARSCHNER, S., MATUSIK, W., AND GROSS, M. 2012. Physical face cloning. *ACM Trans. Graph. 31*, 4 (July), 118:1–118:10.

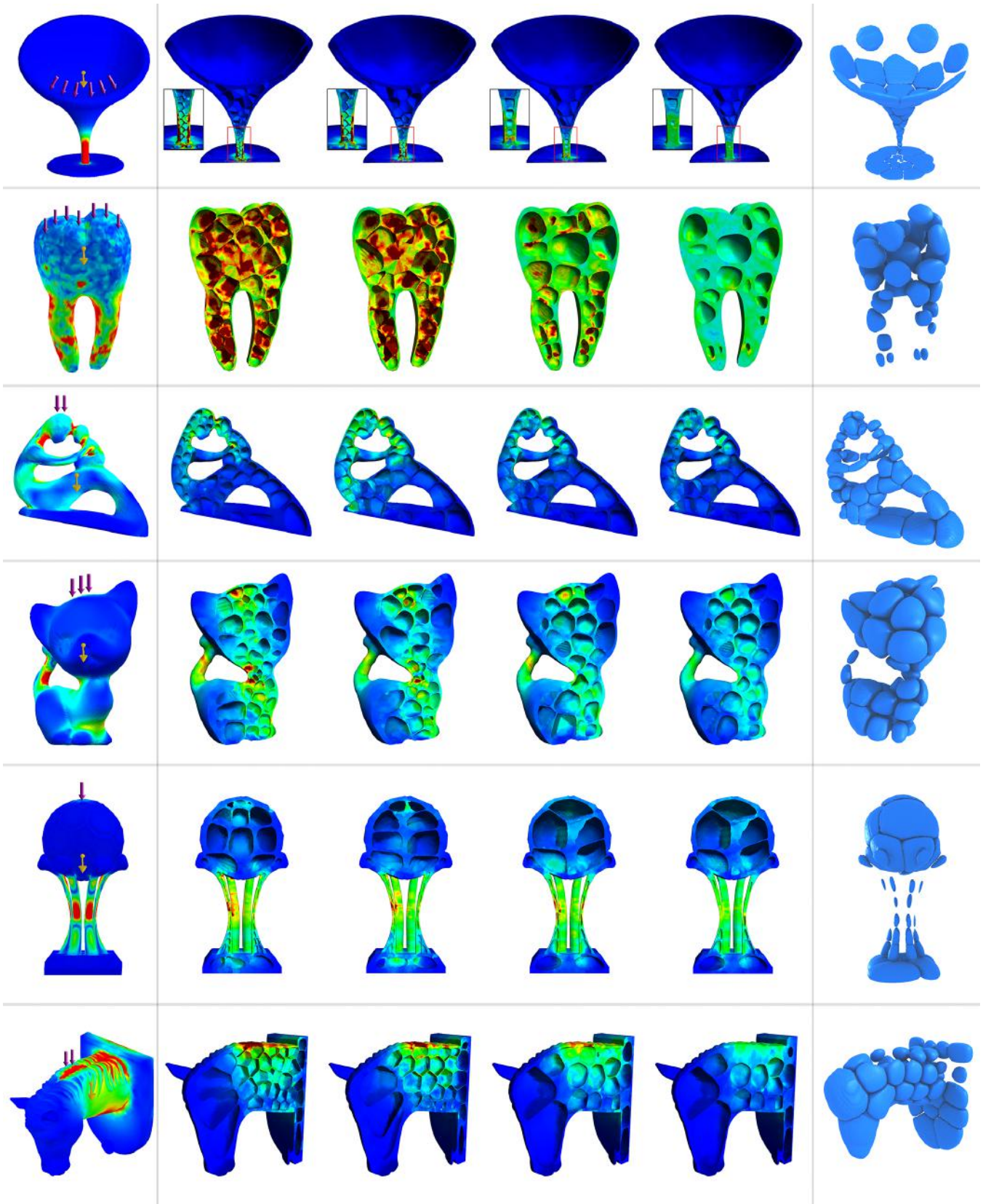

Figure 13: *Build-to-last hollowing results for six different models. Left-to-right, original model with applied forces and initial stress map, three optimization iterations, our optimal strength-to-weight result and rightmost are the resulting 3D porous.*

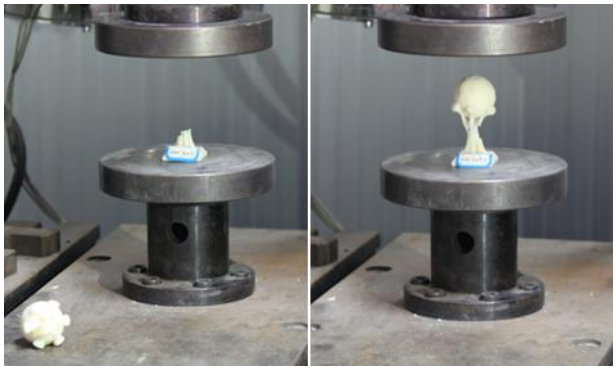

Figure 12: *Compared to an intermediate result (left), our optimal one (right) can sustain higher stress.*

BRONSTEIN, A., BRONSTEIN, M., AND KIMMEL, R. 2008. *Numerical Geometry of Non-Rigid Shapes*, 1 ed. Springer Publishing Company, Incorporated.

CALÌ, J., CALIAN, D. A., AMATI, C., KLEINBERGER, R., STEED, A., KAUTZ, J., AND WEYRICH, T. 2012. 3D-printing of non-assembly, articulated models. *ACM Trans. Graph. 31*, 6 (Nov.), 130:1–130:8.

CEYLAN, D., LI, W., MITRA, N. J., AGRAWALA, M., AND PAULY, M. 2013. Designing and fabricating mechanical automata from mocap sequences. *ACM Trans. Graph. 32*, 6, 186.

CHEN, D., LEVIN, D. I. W., DIDYK, P., SITTHI-AMORN, P., AND MATUSIK, W. 2013. Spec2fab: A reducer-tuner model for translating specifications to 3D prints. *ACM Trans. Graph. 32*, 4, 135:1–135:10.

COROS, S., THOMASZEWSKI, B., NORIS, G., SUEDA, S., FORBERG, M., SUMNER, R. W., MATUSIK, W., AND BICKEL, B. 2013. Computational design of mechanical characters. *ACM Trans. Graph. 32*, 4 (July), 83:1–83:12.

CRAPO, H., AND WHITELEY, W. 1993. The geometry of rigid structures. *Encyclopedia of Math., Cambridge University Press*.

CRAPO, H. 1979. Structural rigidity. *Structural Topology 1*, 26–45.

DU, Q., FABER, V., AND GUNZBURGER, M. 1999. Centroidal voronoi tessellations: Applications and algorithms. *SIAM Review 41*, 4, 637–676.

HAFTKA, R. T., AND GRANDHI, R. V. 1986. Structural shape optimization - a survey. *Computer Methods in Applied Mechanics and Engineering 57*, 1, 91 – 106.

HOLLISTER, S. 2005. Porous scaffold design for tissue engineering. *Nat. Mater. 4*, 7, 518–524.

KHODA, A., OZBOLAT, I. T., AND KOC, B. 2013. Designing heterogeneous porous tissue scaffolds for additive manufacturing processes. *Computer-Aided Design 45*, 12, 1507 – 1523.

KINDINGER, J. 2001. Lightweight structural core. *ASM Handbook 21*, 180–183.

KOU, X., AND TAN, S. 2010. A simple and effective geometric representation for irregular porous structure modeling. *Computer-Aided Design 42*, 10, 930 – 941.

LI, X., GUO, X., WANG, H., HE, Y., GU, X., AND QIN, H. 2007. Harmonic volumetric mapping for solid modeling applications. In *Proceedings of the 2007 ACM Symposium on Solid and Physical Modeling*, ACM, New York, NY, USA, SPM '07, 109–120.

LI, H., VOUGA, E., GUDYM, A., LUO, L., BARRON, J. T., AND GUSEV, G. 2013. 3D self-portraits. *ACM Trans. Graph. 32*, 6 (November).

LLOYD, S. P. 1982. Least squares quantization in PCM. *IEEE Transactions on Information Theory 28*, 2, 129–136.

PATZAK, B., AND RYPL, D. 2012. Object-oriented, parallel finite element framework with dynamic load balancing. *Adv. Eng. Softw.*, 35–50.

POTTMANN, H. 2012. Freeform architecture and fabrication-aware design. *Computers & Graphics 36*, 5 (Aug.).

PRÉVOST, R., WHITING, E., LEFEBVRE, S., AND SORKINE-HORNUNG, O. 2013. Make it stand: balancing shapes for 3D fabrication. *ACM Trans. Graph. 32*, 4 (July), 81:1–81:10.

RIVERS, A., MOYER, I. E., AND DURAND, F. 2012. Position-correcting tools for 2d digital fabrication. *ACM Trans. Graph. 31*, 4 (July), 88:1–88:7.

ROSENBERG, I. 1980. Structural rigidity i: Foundations and rigidity criteria. In *Combinatorics 79 Part I*, M. Deza and I. Rosenberg, Eds., vol. 8 of *Annals of Discrete Mathematics*. Elsevier, 143 – 161.

SCHROEDER, C., REGLI, W. C., SHOKOUFANDEH, A., AND SUN, W. 2005. Computer-aided design of porous artifacts. *Computer-Aided Design 37*, 3, 339 – 353.

SI, H., 2007. Tetgen. a quality tetrahedral mesh generator.

SKOURAS, M., THOMASZEWSKI, B., BICKEL, B., AND GROSS, M. 2012. Computational design of rubber balloons. *Comp. Graph. Forum 31*, 2pt4 (May), 835–844.

SKOURAS, M., THOMASZEWSKI, B., COROS, S., BICKEL, B., AND GROSS, M. 2013. Computational design of actuated deformable characters. *ACM Trans. Graph. 32*, 4 (July), 82:1–82:10.

STAVA, O., VANEK, J., BENES, B., CARR, N., AND MĚCH, R. 2012. Stress relief: improving structural strength of 3D printable objects. *ACM Trans. Graph. 31*, 4 (July), 48:1–48:11.

TELEA, A., AND JALBA, A. 2011. Voxel-based assessment of printability of 3D shapes. In *Proceedings of the 10th international conference on Mathematical morphology and its applications to image and signal processing*, Springer-Verlag, ISMM'11, 393–404.

UMETANI, N., AND SCHMIDT, R. 2013. Cross-sectional structural analysis for 3d printing optimization. In *SIGGRAPH Asia 2013 Technical Briefs*, ACM, New York, NY, USA, SA '13, 5:1–5:4.

VIDIMČE, K., WANG, S.-P., RAGAN-KELLEY, J., AND MATUSIK, W. 2013. Openfab: a programmable pipeline for multi-material fabrication. *ACM Trans. Graph. 32*, 4 (July), 136:1–136:12.

VORONOI, G. 1908. Nouvelles applications des paramètres continus à la théorie des formes quadratiques. deuxième mémoire. recherches sur les p arallélloèdres primitifs. *Journal für die reine und angewandte Mathematik (Crelles Journal) 1908*, 134 (Jan.), 198–287.

WANG, W., WANG, T. Y., YANG, Z., LIU, L., TONG, X., TONG, W., DENG, J., CHEN, F., AND LIU, X. 2013. Cost-effective

printing of 3D objects with skin-frame structures. *ACM Trans. Graph. 32*, 5.

WICKE, M., BOTSCH, M., AND GROSS, M. 2007. A finite element method on convex polyhedra. *Comp. Graph. Forum 26*, 3, 355–364.

WILSON, S. 1990. A new face of aerospace honeycomb. *Materials & Design 11*, 6, 323 – 326.

YAN, D.-M., WANG, W., LÉVY, B., AND LIU, Y. 2013. Efficient computation of clipped voronoi diagram for mesh generation. *Computer-Aided Design 45*, 4, 843 – 852. Geometric Modeling and Processing 2010.

ZHOU, Q., PANETTA, J., AND ZORIN, D. 2013. Worst-case structural analysis. *ACM Trans. Graph. 32*, 4 (July), 137:1–137:12.

ZHU, L., XU, W., SNYDER, J., LIU, Y., WANG, G., AND GUO, B. 2012. Motion-guided mechanical toy modeling. *ACM Trans. Graph. 31*, 6 (Nov.), 127:1–127:10.